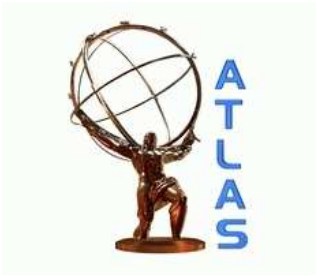

ATLAS NOTE

ATL-PHYS-PUB-2009-000

June 8, 2009

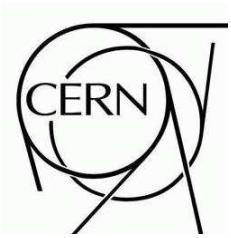

ATLAS searches for MSSM Higgs bosons decaying into SUSY cascades

The ATLAS Collaboration

ATL-PHYS-PUB-2009-079
10 June 2009

Abstract

The neutral MSSM Higgs boson production and subsequent decay into heavy neutralino/chargino pairs has been studied for the ATLAS experiment. The final state with four leptons and missing energy is considered. The study has been performed using a realistic detector simulation of the signal and the SM and MSSM backgrounds for four benchmark scenarios. The discovery and exclusion sensitivity in the (m_A, tanβ) plane was discussed for different luminosity scenarios. An extension of the searches to the charged Higgs boson sector was explored.

1 Introduction

The Minimal Supersymmetric Standard Model (MSSM) is the most investigated extension of the Standard Model (SM). The theory requires two Higgs doublets giving origin to five Higgs bosons: two neutral scalars, h and H (h is the lighter of the two), one neutral pseudoscalar, A, and one pair of charged Higgs bosons, $H^{\pm}$. Their discovery is an irrefutable proof for physics beyond the SM. This is a key point in the physics program of future accelerators and in particular of the LHC. After the conclusion of the LEP program in the year 2000, the experimental limit on the mass of the Standard Model Higgs boson was established at 114.4 GeV with 95% CL [1]. Limits were also set on the mass of neutral [2] and charged [3] MSSM Higgs bosons for most of the representative sets of model parameters.

To achieve an uncontroversial proof of the existence of models beyond SM, the discovery of the heavier bosons H and A is demanded, since the light h boson is indistinguishable from the SM Higgs boson. Many signatures of MSSM neutral Higgs bosons have been studied involving decays into known SM particles, e.g. τ or μ pairs and $b\bar{b}$, by ATLAS [4, 5] and CMS experiments [6], in a scenario where it is assumed that sparticles are too heavy to participate in the process.

If the MSSM Higgs decay into sparticles is kinematically allowed, decay channels involving neutralinos ($\tilde{\chi}^0$), charginos ($\tilde{\chi}^{\mp}$) and sleptons ($\tilde{\ell}$) can be considered, enlarging the possibilities of discovery. The decay of neutral [7–9] and charged Higgs bosons [8, 10] into neutralinos and charginos and the subsequent decay into sleptons have been studied. The focus of these works is on neutral Higgs bosons decaying into four leptons via $\tilde{\chi}_2^0\tilde{\chi}_2^0$. In Ref. [11] the decay into a heavier neutralino pair as well as a chargino pair are taken into account, extending the discovery reach. A recent study has included decays of charged Higgs bosons [12].

The unconstrained MSSM has a large number of parameters (105) in addition to the SM ones (19), making any phenomenological analysis very complicated. The number of parameters is reduced to about twenty with the assumptions mentioned in Section 2. In the following we refer shortly to this constrained model as MSSM. In a further simplified version (mSUGRA) with additional assumptions about unification at some GUT (Grand Unification Theory) scale, the number of parameters is reduced to five.

In this paper, following closely Ref. [11], we discuss the potential of the ATLAS detector at LHC for the discovery of neutral supersymmetric Higgs bosons, considering the decays of A/H into neutralino and chargino pairs, with subsequent decay into lighter neutralinos and leptons, Fig. 1, and an experimental final state signature of four leptons and missing energy (due to the presence of $\tilde{\chi}_1^0$-s). An extension to the charged Higgs boson sector is also discussed. The analysis is performed in four different scenarios, two for MSSM and two for mSUGRA. These scenarios in general also give complementary signatures, that should allow the detection of supersymmetric particles in channels requiring a lower integrated luminosity.

In Section 2, the MSSM and mSUGRA frameworks are shortly introduced. In Section 3, the MSSM and mSUGRA parameters are defined and four reference points are chosen as representative of the analysis; SM and SUSY backgrounds are discussed. In Section 4 the analysis strategy and the results of the scan over the (m_A, $\tan\beta$) plane is described. In the Conclusion, the discovery potential of the ATLAS detector for neutral and charged (MSSM, mSUGRA) Higgs bosons is presented. For a detailed discussion on the Monte Carlo generators, the software tools and the description of the ATLAS detector, we refer to recent ATLAS Collaboration papers [5, 13].

2 Minimal Supersymmetric Standard Model

We mention only few points of the model, as needed for the present analysis, and refer to Refs. [14–18] for a complete review. At tree level, the masses of the five Higgs bosons of the unconstrained MSSM are

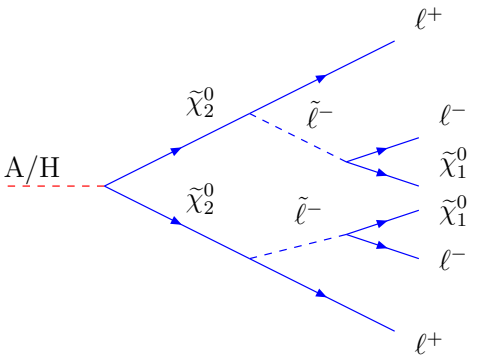

Figure 1: Example of *A*/*H* decay ($A/H \rightarrow \tilde{\chi}_2^0\tilde{\chi}_2^0$) with final state containing four leptons and undetectable particles.

related by the following equations:

$$m_{H,h}^2 = \frac{1}{2}[m_A^2 + m_Z^2 \pm \sqrt{(m_A^2 + m_Z^2)^2 - 4m_A^2 m_Z^2 \cos^2 2\beta}], \tag{1}$$

$$m_{H^\pm}^2 = m_W^2 + m_A^2,$$

where m_W and m_Z are the W and Z mass, respectively, and tanβ is the ratio of the vacuum expectation values of the two Higgs fields. At tree level, the same parameters (m_A, tanβ) enter into the evaluation of the Higgs bosons coupling to SM particles and their cross sections.

In the general case of unconstrained MSSM a large number of parameters is introduced to allow the intergenerational mixing and complex phases [14]. A phenomenological MSSM can be defined with additional assumptions, for instance: a) no new source of CP-violation in addition to the one of CKM matrix; b) flavour conservation in neutral current at tree level; c) the soft SUSY-breaking masses and the trilinear couplings of the first and second sfermions generations are the same at low energy. Based on these assumptions the number of parameters can be reduced to about twenty. This model with a relatively moderate number of parameters is more predictive and is easier to investigate; as mentioned in the Introduction we refer to it simply as MSSM.

A further reduction of the number of parameters is obtained with the unification of the gauge coupling constants (Grand Unification at $\sim 2 \cdot 10^{16}$ GeV), indicated by LEP data, and also by imposing the unification of gaugino (bino, wino, gluino) masses, of the universal scalar (sfermion and Higgs boson) masses and of the universal trilinear couplings. The model adopting these specific assumptions, mSUGRA, is defined by five parameters. In both MSSM and mSUGRA scenarios the lightest SUSY particle is the lightest neutralino, $\tilde{\chi}_1^0$.

3 MSSM and mSUGRA model parameters for Higgs bosons decaying into SUSY cascades

As mentioned above, we study the decay processes involving light neutralinos, $A/H \rightarrow \tilde{\chi}_2^0\tilde{\chi}_2^0$, heavier neutralinos, *A*/*H*$\rightarrow \tilde{\chi}_2^0\tilde{\chi}_3^0$, $\tilde{\chi}_2^0\tilde{\chi}_4^0$, $\tilde{\chi}_3^0\tilde{\chi}_3^0$, $\tilde{\chi}_3^0\tilde{\chi}_4^0$, $\tilde{\chi}_4^0\tilde{\chi}_4^0$, and chargino states, $A/H \rightarrow \tilde{\chi}_1^\pm\tilde{\chi}_2^\pm$,$\tilde{\chi}_2^+\tilde{\chi}_2^-$, with the subsequent $\tilde{\chi}_2^0 \rightarrow \tilde{\chi}_1^0\ell^+\ell^-$ decay. All these processes lead to a final state of four leptons and missing

energy. The parameters, in MSSM and mSUGRA framework, have been chosen with the purpose of maximising the detection probability of these processes, e.g. by enhancing the leptonic branching ratio; see Ref. [11] for an exhaustive discussion.

MSSM

In the following we denote by M_1 and M_2 the gaugino masses; μ, the strength of the supersymmetric Higgs boson mixing; $m_{\tilde{g}}$, the gluino mass; $m_{\tilde{q}}$, the $\tilde{q}$ masses; $m_{\tilde{\ell}}$ and $m_{\tilde{\tau}}$, the slepton and stau masses.

The Higgs boson decays into $\tilde{\chi}_2^0\tilde{\chi}_2^0$ are the dominant source of signal events in the regions with low M_2 values and moderate to high $|\mu|$ values. For low to moderate M_2 values and $|\mu|$ low values, the dominant source of signal events is the decay into heavier neutralinos or charginos. Based on these considerations two sets of parameter values have been selected for the MSSM parameter space [11, 19]:

- **Set1**: M_1 = 90 GeV, M_2 = 180 GeV, μ = -500 GeV,
  $m_{\tilde{\ell}\text{soft}}$= $m_{\tilde{\tau}\text{soft}}$=250 GeV, $m_{\tilde{g}}$=$m_{\tilde{q}}$= 1000 GeV,
- **Set2**: M_1 = 100 GeV, M_2 = 200 GeV, μ = -200 GeV,
  $m_{\tilde{\ell}\text{soft}}$= 150 GeV, $m_{\tilde{\tau}\text{soft}}$=250 GeV, $m_{\tilde{g}}$= 800 GeV, $m_{\tilde{q}}$=1000 GeV,

where $m_{\tilde{\ell}\text{soft}} \equiv m_{\tilde{\ell}_{L,R}}$, and the generation couplings are set to A_τ=A_ℓ=0.The gaugino mass M_1 is determined from the M_2 gaugino mass via gaugino unification (M_1= $\frac{5}{3}\sin^2\theta_W M_2$).

Because of the choice of M_2 and μ values, Set1 is representative of a region where most of the signal is produced via $A/H \rightarrow \tilde{\chi}_2^0\tilde{\chi}_2^0$; Set2 corresponds to a region where the signal comes from heavier -inos, $A/H \rightarrow \tilde{\chi}_2^0\tilde{\chi}_3^0$, $\tilde{\chi}_2^0\tilde{\chi}_4^0$, $\tilde{\chi}_3^0\tilde{\chi}_3^0$, $\tilde{\chi}_3^0\tilde{\chi}_4^0$, $\tilde{\chi}_4^0\tilde{\chi}_4^0$ and $A/H \rightarrow \tilde{\chi}_1^\pm\tilde{\chi}_2^\pm$, $\tilde{\chi}_2^+\tilde{\chi}_2^-$.

It should be noted, also, the difference in slepton parameters. Soft slepton masses for all three generations are degenerate in Set1; the stau mass is well above the other slepton masses in Set2.

For each set, a point has been chosen as representative to discuss the analysis procedure:

- **Point1**: m_A=500 GeV and tanβ=20, in Set1,
- **Point2**: m_A= 600 GeV and tanβ=35, in Set2.

Then a scan is performed in the (m_A, tanβ) plane.

mSUGRA

Including additional assumptions on the unification of SUSY at very high mass scale (GUT), Section 2, the free parameters are reduced to tanβ, $m_{1/2}$ (the universal gaugino mass), m_0 (the universal sfermion mass), A_0 (the universal trilinear coupling), and the sign of μ ($|\mu|$ is not a free parameter, but is connected to the masses of scalar Higgs bosons via the m_0 input). In this framework the parameter set chosen are:

- **SetA**: m_0= 400 GeV, $m_{1/2}$=165 GeV, sgn(μ) =+1, A_0=0,
- **SetB**: m_0= 125 GeV, $m_{1/2}$=165 GeV, sgn(μ) =+1, A_0=0.

For each set a point has been chosen as representative to discuss the analysis procedure:

- **PointA**: tanβ=20 in SetA,
- **PointB**: tanβ=20 in SetB.

The values obtained for the gluino masses are $m_{\tilde{g}}$= 422 GeV and $m_{\tilde{g}}$= 438 GeV for PointA and PointB, respectively. The values obtained for the $\tilde{q}$ masses $m_{\tilde{q}}$ are in the range between 298 to 382 GeV for PointA and between 358 to 526 GeV for PointB, depending on flavour. In SetA the signal is dominated by $A/H \to \tilde{\chi}_2^0\tilde{\chi}_2^0$ decays; with SetB includes a large contribution from heavier -inos. The study is performed as a function of tanβ, corresponding to m_A = 257 GeV (PointA) and m_A = 439 GeV (PointB). The relevant sparticle masses for these MSSM and mSUGRA parameter points, reported in Table 1, as well as the decay rates, are determined by ISAJET7.75 [19].

Table 1: The relevant sparticle masses for Point1, Point2 (MSSM) and PointA, PointB (mSUGRA) (see Section 5).

	Point1	**Point2**	**PointA**	**PointB**
Particle	m[GeV]	m[GeV]	m[GeV]	m[GeV]
A	500.0	600.0	257.4	439.5
H	503.4	603.9	259.1	442.5
$\tilde{\chi}_1^0$	89.7	93.9	61.1	62.3
$\tilde{\chi}_2^0$	176.3	155.5	109.4	111.9
$\tilde{\chi}_3^0$	507.0	211.9	235.9	241.9
$\tilde{\chi}_4^0$	511.0	262.6	259.8	265.4
$\tilde{\chi}_1^\pm$	176.3	153.1	108.7	111.6
$\tilde{\chi}_2^\pm$	514.0	263.6	260.2	265.9

4 Signal and background production

The Higgs boson production modes considered herein are $gg \to H/A$ (gluon-fusion) and $q\bar{q} \to H/A$ (quark-fusion). A detailed discussion can be found in Ref. [11]. Other processes, in Standard Model and in MSSM(mSUGRA), with the same final state as the signal, four leptons and missing energy, are considered background. The Standard Model background originates from the production of a Z pair or a $t\bar{t}$ pair or a Z accompanied by a $b\bar{b}$ pair.

The MSSM (mSUGRA) background originates from squark or gluino ($\tilde{q}$,$\tilde{g}$) pair production, from slepton ($\tilde{\ell}$,$\tilde{\nu}$) pair production, from direct neutralino/chargino ($\tilde{\chi}\tilde{\chi}$, $\tilde{q}/\tilde{g}\tilde{\chi}$) production and charged Higgs ($tH^\pm$). The amount of background depends on the point considered in the (m_A, tanβ) plane.

Since the background processes have production cross-sections much higher than the signal, in order to disentangle the signal from the background, an excellent performance in the lepton, μ and e, detection is required, as well as a high quality measurement of the missing transverse energy, $E_{\mathrm{T}}^{\mathrm{miss}}$.

5 Monte Carlo samples

The event samples used in this analysis follow the recommendations in Ref. [5]. A detailed account of the procedures, generators and settings used is given therein. Simulation, digitalization and reconstruction are all performed within the ATLAS software framework ATHENA [5], where the ATLAS detector is simulated by GEANT4 [20].

We have generated, at a center-of-mass energy $\sqrt{s}$ = 14 TeV, MSSM (mSUGRA) signal and background events, for an integrated luminosity $\int \mathscr{L}\,\mathrm{d}t$ = 300 fb^{-1}, as well as Standard Model background

events, as in Ref. [5]. Out of the Standard Model background processes, two ($Zb\bar{b}$ and ZZ) were produced at this same luminosity, thus with a statistics which is many times the signal full statistics. The number of $t\bar{t}$ events generated corresponds, instead, to $\approx \frac{1}{3}$ that luminosity.

The MSSM signal processes were generated in the (m_A, tanβ) plane in the interval 5 - 50 for tanβ (in steps of 5) and 375 - 900 GeV for m_A (in steps of 250 GeV) for Set1 and Set2 [1)].

The mSUGRA signal processes were generated in the interval 5 - 50 for tanβ (in steps of 5) that corresponds to a m_A value in the interval (190 - 291) GeV in SetA, and (247 - 497) GeV in SetB [2)].

Some of the supersymmetric background processes ($tH^{\pm}$ for MSSM; ($\tilde{\ell}$,$\tilde{\nu}$) and ($\tilde{\chi}\tilde{\chi}$, $\tilde{q}/\tilde{g}$ $\tilde{\chi}$) for mSUGRA) were generated at each point of the scan. Others (($\tilde{q}$,$\tilde{g}$), ($\tilde{\ell}$,$\tilde{\nu}$) and ($\tilde{\chi}\tilde{\chi}$, $\tilde{q}/\tilde{g}$ $\tilde{\chi}$) for MSSM; ($\tilde{q}$,$\tilde{g}$) for mSUGRA), due to their negligible dependence on m_A, were produced only for the reference points. Both in MSSM and mSUGRA scenarios, the gluino and squark masses do not vary significantly ($< 10^{-3}$ in SetA), so the rates of squark and gluino production are nearly constant. The -ino masses change also very slightly ($\leq 1\%$ in Set2 and SetA).

The mass spectra and decay tables from ISAJET7.75 [19] were used via HERWIG/JIMMY6.5 [21, 22] to generate the signal and sparticle cascade decays, the supersymmetric backgrounds, the parton showers and underlying events, as in Ref. [5], using a mass value of 175 GeV and 4.25 GeV for t and b quark, respectively.

The Standard Model background events were generated as follows: $t\bar{t}$ with MC@NLO3.1 [23]; ZZ with PYTHIA6.3 [24]; $Zb\bar{b}$ with ACERMC3.1 [25]. The samples used are those of Ref. [5]. Corrections were applied as in Ref. [5]; the QCD ZZ cross section was increased by 30% to account for a missing box diagram in PYTHIA6.3; 8.64 pb (15%) was added to the $Zb\bar{b}$ cross-section to account for the $q\bar{q} \rightarrow Zb\bar{b}$ diagrams that are not included in the generation. We note that in ZZ, $Zb\bar{b}$ samples the full Z/γ^* interference is taken into account. In the $Zb\bar{b}$ sample a cut on requiring the invariant mass of lepton pair from Z/γ to be greater than 30 GeV is applied. A delicate point of this analysis may arise from limited precision of b-quark fragmentation function; that is dealt with in Ref. [5]. All cross sections used were calculated at leading-order (LO) except for the $gg \rightarrow ZZ$ box-diagram contribution (47.64 fb); the $t\bar{t}$ cross section was assumed to be at the same level of precision.

During the generation, a filter was applied to the samples, requiring four leptons with $p_{\mathrm{T}} > 5$ GeV within an acceptance $|\eta| < 2.7$ for the pseudorapidity η. Accordingly, an effective branching ratio $\mathrm{Br} \times \varepsilon$ was defined, where Br is the four lepton branching ratio and ε generation filter. Additional backgrounds where one or more of the reconstructed leptons is a fake are ignored in this analysis. Fake muons could arise from punch through and are expected to be small, fake electrons could arise from misidentified jets or pions from τ decays. The soundness of this approximation is based on the conclusions of Ref. [5] updated for present analysis.

Effective generator level rates are shown in Figs. 2 and 3 for MSSM Set1, in Fig. 4 for MSSM Set2, and in Tables 2 and 3.

For MSSM Set1, Fig.2 shows, as a function of m_A the Higgs boson A production cross section σ, on the left, and the effective branching ratio $\mathrm{Br} \times \varepsilon$, on the right. The product $\sigma \times \mathrm{Br} \times \varepsilon$ is shown, as a function of m_A, in Fig. 3, for the Higgs bosons A, top left, and H, top right, and for the MSSM backgrounds, ($\tilde{q}$,$\tilde{g}$), ($\tilde{\ell}$,$\tilde{\nu}$), ($\tilde{\chi}\tilde{\chi}$, $\tilde{q}/\tilde{g}$ $\tilde{\chi}$), bottom left, and ($tH^{\pm}$), bottom right. The contribution of $tH^{\pm}$ decays is negligible in Set1.

For MSSM Set2, Fig. 4 shows, as a function of m_A, the product $\sigma \times \mathrm{Br} \times \varepsilon$ for the Higgs boson A, on the left, and for $tH^{\pm}$, on the right. The contribution of $tH^{\pm}$ decays is not negligible in Set2.

Table 2 shows for the MSSM and mSUGRA events at the reference points, from left to right, the process considered (either signal or background), the corresponding cross section σ at LO, the four lepton effective branching ratio $\mathrm{Br} \times \varepsilon$, the number of events expected for $\int \mathscr{L}\,\mathrm{d}t$ = 300 fb^{-1}, $\mathrm{N}_{300}^{\mathrm{exp}}$,

[1)] The Set1 scan includes tanβ = 8 and is limited by lack of signal statistics to tanβ = 35. The Set2 scan includes tanβ = 3.

[2)] The SetA scan is limited to tanβ = 44.

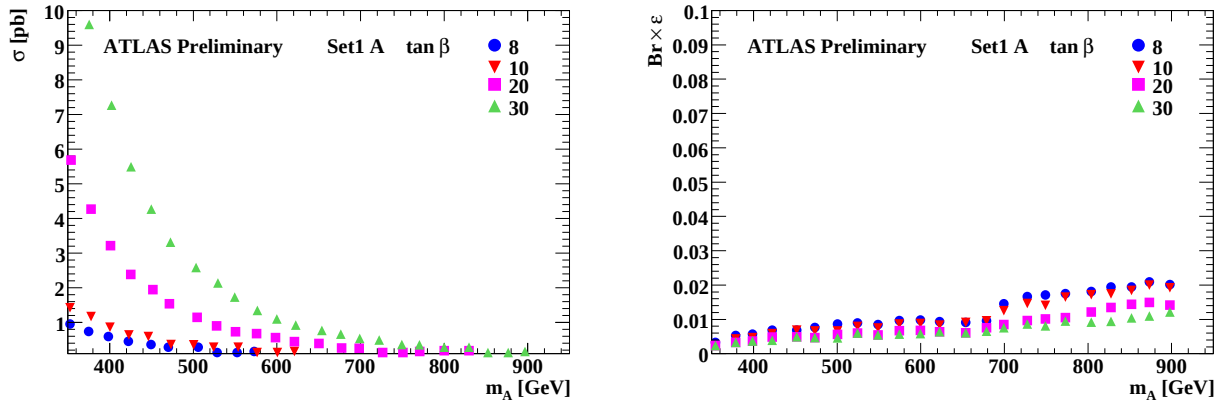

Figure 2: Results at the generator level for **Set1**, as a function of m_A, at tanβ = 8, 10, 20, 30. On the left, the Higgs boson A production cross section σ. On the right, the effective four lepton branching ratio, Br $\times$ ε (see text).

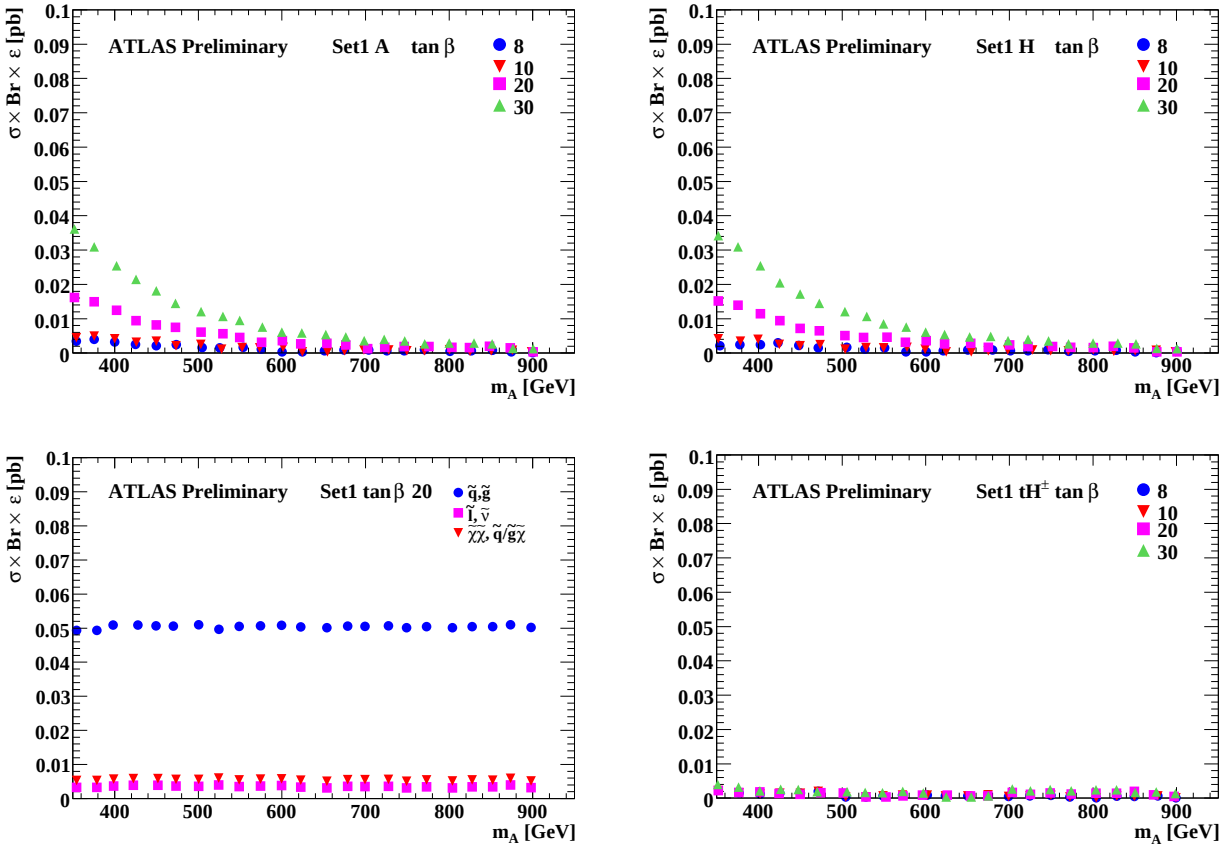

Figure 3: Results at the generator level for **Set1**, as a function of m_A, at tanβ = 8, 10, 20, 30: the production cross section σ times the four lepton effective branching ratio Br $\times$ ε for A events (top left); H events (top right); ($\tilde{q}$,$\tilde{g}$), ($\tilde{\ell}$,$\tilde{\nu}$), ($\tilde{\chi}\tilde{\chi}$, $\tilde{q}/\tilde{g}\,\tilde{\chi}$) events (bottom left); $tH^{\pm}$ events (bottom right).

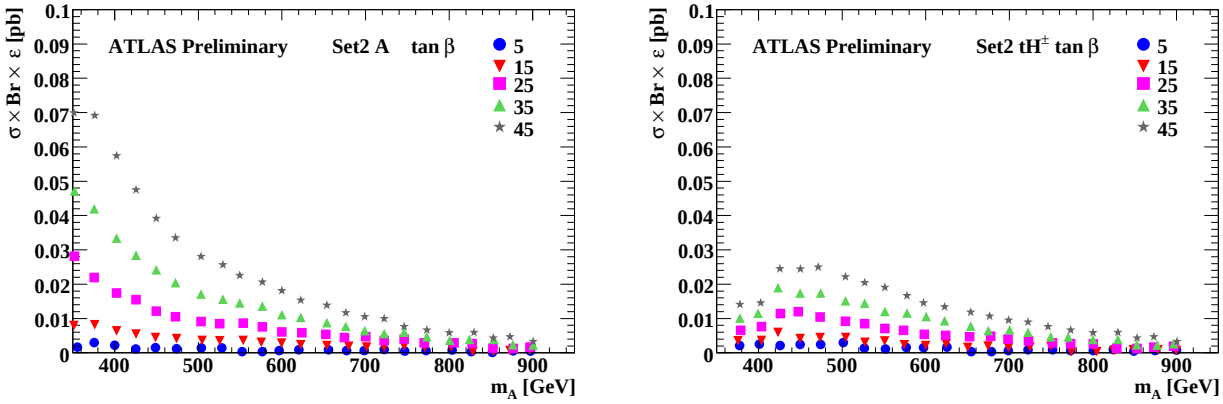

Figure 4: Results at the generator level for **Set2**, as a function of m_A, at tanβ = 5, 15, 25, 35, 45: the production cross section σ times the four lepton effective branching ratio Br $\times\, \varepsilon$ for A events (left); $tH^{\pm}$ events (right).

and the number of events generated, N^{MC}. In Table 3 the same type of information is reported for the Standard Model background.

Table 2: Monte Carlo samples at the two reference points for MSSM (Point1, Set1 and Point2, Set2) and for mSUGRA (PointA, SetA and PointB, SetB). From left to right: reference point, process source, σ (LO cross section), Br $\times\, \varepsilon$ (effective branching ratio), N^{exp}_{300} (number of expected events for $\int \mathscr{L}\, dt = 300$ fb^{-1}) and N^{MC} (number of generated events).

	Process	σ [pb]	Br $\times\, \varepsilon$	N^{exp}_{300}	N^{MC}		σ [fb]	Br $\times\, \varepsilon$	N^{exp}_{300}	N^{MC}
Point1	A	1.18	0.0051	1810	2250	**Point2**	1.52	0.0078	3550	5250
	H	1.16	0.0049	1730	2500		1.49	0.0076	3415	5000
	$\tilde{q}$,$\tilde{g}$	1.49	0.034	15060	17000		2.99	0.14	129300	144000
	$\tilde{\ell}$,$\tilde{\nu}$	0.153	0.024	1110	1500		0.771	0.00073	170	500
	$\tilde{\chi}\tilde{\chi}$, $\tilde{q}/\tilde{g}\ \tilde{\chi}$	2.97	0.0019	1730	2500		4.21	0.0036	4520	6250
	$tH^{\pm}$	0.136	0.0078	315	500		0.22	0.048	3150	3750
PointA	A	20.7	0.0015	9500	12250	**PointB**	2.12	0.0031	1970	3725
	H	21.3	0.0015	9580	16250		2.11	0.0036	2260	4750
	$\tilde{q}$,$\tilde{g}$	216	0.014	934000	440250		98.8	0.015	432000	470050
	$\tilde{\ell}$,$\tilde{\nu}$	783	0.016	3740	4750		0.0197	0.017	100	500
	$\tilde{\chi}\tilde{\chi}$, $\tilde{q}/\tilde{g}\ \tilde{\chi}$	20.3	0.0033	20150	22750		15.5	0.0013	6120	7945
	$tH^{\pm}$	0.784	0.017	3980	6500		0.203	0.028	1690	3500

All the events generated within the acceptance of the generation filter were fully simulated as discussed above. The efficiency of the selection criteria, the detector acceptance and the purity of the data sample are estimated from these fully simulated events.

Table 3: Monte Carlo samples for Standard Model background. From left to right: process, σ (LO cross section), Br $\times \varepsilon$ (effective branching ratio), N_{300}^{exp} (number of expected events for $\int \mathscr{L} dt$ = 300 fb^{-1}) and N^{MC} (number of generated events). For ZZ, $\ell = e, \mu, \tau$, otherwise $\ell = e, \mu$. The relative errors on Br $\times \varepsilon$ are smaller than 0.4 %. In the first row the second term of cross section is explained in the text. The meaning and use of negative weights shown in the last row is given in Ref. [23]. They are necessary in order to obtain the exact results for total rate and differential distributions for $t\bar{t}$ process.

Process	σ [fb]	Br $\times \varepsilon$	N_{300}^{exp}	N^{MC}
$q\bar{q} \to ZZ \to 4\ell$	158.8 + 47.64	0.219	13600	115700
$gg \to Zb\bar{b} \to 4\ell$	52030	0.00942	170970	438900
$q\bar{q} \to Zb\bar{b} \to 4\ell$	8640			
$gg, q\bar{q} \to t\bar{t}$	500000	0.00728	1092000	394400
$t\bar{t}$ (negative weight)				52930

6 Event reconstruction

A detailed description of the reconstruction of simulated events can be found in [5], particularly for the key objects of the analysis: muons and electrons. In ATLAS, the muon reconstruction is performed by combining the information from the muon spectrometer, the inner detector and the calorimeters. The software associates segments and tracks found in the spectrometer with the corresponding inner detector tracks, so to identify muons at their production vertex with an optimum resolution. Electron candidates are formed from clusters of cells in the electromagnetic calorimeter accompanied by a matched track. The electron identification takes also into account the shape of the shower and the tracking information.

In addition to the standard lepton identification, we require that the sum of the transverse energies deposited in an isolation cone of radius ΔR be less than 6 GeV, where $\Delta R = \sqrt{\Delta\eta^2 + \Delta\phi^2} = 0.2$, η being the pseudorapidity and ϕ the polar angle around the lepton direction.

The calorimeter jets are not a primary characteristic of the signal. Yet, with a view to evaluate the energy of the partons produced in the original collision, they are reconstructed using a seed fixed-cone algorithm with a cone size ΔR = 0.4 [5]. Cuts on ${p_T}^{jet} > 20$ GeV and $|\eta| < 2.7$ are initially applied. The signal can be efficiently triggered by a single high-p_T lepton trigger requiring a 20 GeV muon or an isolated 22 GeV electron. The efficiency of this trigger was studied on an unbiased sample of signal events (at the generator level $p_T >$ 5 GeV within an acceptance $|\eta| < 2.7$). The mean efficiency was estimated to be $\approx$ 95.5 %. The trigger losses were shown to be negligible, as expected, by studying the signal events after their selection, Section 8.

7 Event selection

In order to obtain evidence for the signal, it is necessary to discriminate it from background events containing four leptons (e or μ) and transverse missing energy. This goal may be achieved with the following selection criteria:

1 Preselection :

- Trigger: one isolated electron with $p_T >$ 22 GeV or one muon with $p_T >$ 20 GeV, in the pseudorapidity range $|\eta| < 2.5$.
- Four leptons with transverse momentum ${p_T}^{\ell} > 5$ GeV, in the pseudorapidity range $|\eta| < 2.5$.
- Lepton isolation (Section 6): $\Sigma p_T < 6$ GeV in a cone $\Delta R =$ 0.2 .

- Two pairs of opposite sign, same flavor leptons (the four leptons can have all the same flavor) ($\ell_a^-\ell_a^+, \ell_b^-\ell_b^+$) or ($\ell_a^-\ell_a^+, \ell_a^-\ell_a^+$).

2 Impact parameter significance:

- $d0/\sigma_{d0} < 6$ for electron, < 4 for muon.

3 Dilepton invariant mass, $M_{\rm inv}^{\ell\ell}$:

- $|M_{\rm inv}^{\ell\ell} - m_Z| > 6$ GeV.

4 Missing transverse energy, $E_{\rm T}^{\rm miss}$:

- 35 GeV $< E_{\rm T}^{\rm miss} <$ 130 GeV (Set1, Set2, SetB).
- 35 GeV $< E_{\rm T}^{\rm miss} <$ 110 GeV (SetA).

5 Lepton transverse momentum, ${p_{\rm T}}^{\ell}$ (${p_{\rm T}}^{\ell}{}_1$, ${p_{\rm T}}^{\ell}{}_2$ are the first and second largest ${p_{\rm T}}^{\ell}$):

- ${p_{\rm T}}^{\ell} > 8$ GeV.
- 25 GeV $< {p_{\rm T}}^{\ell}{}_1 <$ 110 GeV.
- ${p_{\rm T}}^{\ell}{}_1 <$ 100 GeV and ${p_{\rm T}}^{\ell}{}_2 <$ 55 GeV (Set1, Set2, SetB).
- ${p_{\rm T}}^{\ell}{}_1 <$ 60 GeV and ${p_{\rm T}}^{\ell}{}_2 <$ 40 GeV (SetA).
- ${p_{\rm T}}^{\ell}{}_2 >$ 15 GeV (Set2, SetA).

6 Number and transverse momentum of jets, N^{jet}, ${p_{\rm T}}^{jet}$ with $|\eta| < 2.5$:

- $N^{jet} \leq 5$, ${p_{\rm T}}^{jet} >$ 20 GeV (Set1, Set2, SetA).
- no jet with ${p_{\rm T}}^{jet} >$ 100 GeV (SetA).
- $N^{jet} \leq 3$, ${p_{\rm T}}^{jet} >$ 30 GeV (SetB).
- no jet with ${p_{\rm T}}^{jet} >$ 120 GeV (SetB).

7 Four lepton invariant mass, $M_{\rm inv}^{\ell\ell\ell\ell}$:

- $M_{\rm inv}^{\ell\ell\ell\ell} <$ 125 GeV (SetA).

The *preselection* cuts demanding four tightly isolated leptons is a powerful requirement in fighting the $t\bar{t}$ and $Zb\bar{b}$ background. Unfortunately this cut reduces also significantly the signal.

The cut on the transverse impact parameter significance of tracks associated to leptons (defined as $d0/\sigma_{d0}$, where $d0$ is the distance of closest approach on transverse plane) allows the signal to be discriminated from $t\bar{t}$ or $Zb\bar{b}$, since the leptons in these events are mostly originated from displaced vertices. This cut has a limited effect on signal. We note that the electron and muon cuts are different because for electrons, bremsstrahlung smears the impact parameter distribution, hence reducing the discriminating power of this cut with respect to muons.

The cut on the reconstructed invariant mass of each lepton pair is designed to depress the events from the irreducible Z background, ZZ and $Zb\bar{b}$.

The missing transverse energy, $E_{\rm T}^{\rm miss}$, is a clear signature of supersymmetric Higgs bosons decaying into SUSY cascades. A lower limit on $E_{\rm T}^{\rm miss}$ value removes backgrounds from ZZ and $Zb\bar{b}$, not accompanied by undetectable particles. The MSSM (mSUGRA) background processes, in particular direct ($\tilde{q}$,$\tilde{g}$) production, are accompanied by a $E_{\rm T}^{\rm miss}$ larger than in the signal events. An upper limit on $E_{\rm T}^{\rm miss}$ value removes these backgrounds.

Cuts are applied on lepton events with the largest and second largest transverse momentum, ${p_{\mathrm{T}}}^{\ell}{}_1$ and ${p_{\mathrm{T}}}^{\ell}{}_2$, or on their combination, mostly against $t\bar{t}$ and ($\tilde{q}$,$\tilde{g}$) processes. The squark/gluino production ($\tilde{q}$,$\tilde{g}$) is characterized by a large jet multiplicity and jet transverse momentum. A selection on number of jets and jet transverse momentum is applied for this purpose. The cut on four leptons invariant mass is effective to disentangle signal from background only for SetA.

Other selection criteria could be considered as for example to exploit the isolation of leptons. In the signal they are equally isolated, in turn in $t\bar{t}$ background it is not likely that the two leptons of the same charge are the most isolated pair in the event.

Results from these selections, including the distributions of the most significant variables at different steps of the analysis, are reported in Section 8 for each reference point.

8 Selection results at reference points

The percentage of reconstructed events after each selection step at the MSSM (Point1, Point2) and mSUGRA (PointA, PointB) reference points are summarized in Tables 4, 5, 6, 7. We choose here to discuss, as an example, the MSSM reference point Point2 because of the favorable signal to background ratio and the possibility to search for both neutral and charged MSSM Higgs bosons. For this point, we justify the selection criteria of Section 7 by showing examples of reconstructed distributions obtained for the signal (A, H) and the background (MSSM, ($\tilde{q}$,$\tilde{g}$), ($\tilde{\ell}$,$\tilde{\nu}$), ($\tilde{\chi}\tilde{\chi}$, $\tilde{q}/\tilde{g}\ \tilde{\chi}$), ($tH^{\pm}$)) and Standard Model, ($t\bar{t}$, ZZ, $Zb\bar{b}$), see Figs. 5-9 and Table 5.

The distributions of the lepton impact parameter significance, $d0/\sigma_{d0}$, are displayed in Fig. 5 after cut 1, for muons, in A and $t\bar{t}$ samples, and for electrons, in H and $Zb\bar{b}$ samples. The corresponding selection (cut 2) is extremely effective by reducing the number of events in $t\bar{t}$ and $Zb\bar{b}$ samples to $\sim 0.07\%$ and $\sim 0.9\%$ respectively, with a limited effect on the signal. The reconstructed dilepton invariant mass, $M^{\ell\ell}_{\mathrm{inv}}$, is shown in Fig. 6 after cuts 1-2, for signal (A, H) and background (ZZ, $Zb\bar{b}$). The background events are significantly reduced after cut 3 (ZZ to $\sim 4.3\%$ and $Zb\bar{b}$ to $\sim 0.26\%$).

In Fig. 7 the distributions of $E_{\mathrm{T}}^{\mathrm{miss}}$, after cuts 1-2-3 shows that the signal missing transverse energy is larger than in the ZZ and $Zb\bar{b}$ events, but smaller than in ($\tilde{q}$,$\tilde{g}$) events. Applying cut 4 reduces the events from squark or gluino ($\tilde{q}$,$\tilde{g}$) pair production to $\sim 0.3\%$, from ZZ to $\sim 0.2\%$ and from $Zb\bar{b}$ to $\sim 0.01\%$; the signal is slighly reduced.

Figure 8 shows signal and background ($t\bar{t}$, ($\tilde{q}$,$\tilde{g}$)) distributions of ${p_{\mathrm{T}}}^{\mu}$ and ${p_{\mathrm{T}}}^{e}$, after cuts 1-2-3-4. Cut 5 on the transverse momentum of leptons has a considerable impact on background reduction ($t\bar{t}$ to $\sim 4.8 \cdot 10^{-3}$ and ($\tilde{q}$,$\tilde{g}$) to $\sim 0.06\%$). Figure 9 shows distributions of ${N}^{jet}$ and ${p_{\mathrm{T}}}^{jet}$ after cuts 1-2-3-4-5 for the signal (A, H) and the background ($\tilde{q}$,$\tilde{g}$). Cut 6 reduces to a negligible value the contribution of ($\tilde{q}$,$\tilde{g}$) in the final sample, leaving the signal untouched.

The number of events at the four reference points are given in Table 8 for $\int \mathscr{L}\,\mathrm{d}t = 300\ \mathrm{fb}^{-1}$. We note that at Point2 the main background contributions come from $t\bar{t}$ process (Standard Model) and direct neutralino/chargino ($\tilde{\chi}\tilde{\chi}$, $\tilde{q}/\tilde{g}\ \tilde{\chi}$) and charged Higgs boson $tH^{\pm}$ processes (MSSM). The $tH^{\pm}$ contribution is negligible at the other reference points. This fact indicates that, at Point2, the search could be extended to charged Higgs bosons.

The results for the different reference points, reported in Table 8, indicate that Set1 is less promising than Set2, in MSSM, and that SetB is less promising than Set A in mSUGRA.

Table 4: *Point1 selection results*. From left to right: Process source, cumulative fraction of events (in %) after each (1-6) selection cut, Section 7. For each channel, the fractions of selected events are calculated with respect to the events of each channel, N_{300}^{exp}, given in Tables 2, 3. N_{300}^{exp} are the number of events passing the generation filter described in Section 5.

Process	1	2	3	4	5	6
A	2.93	2.44	2.31	1.87	1.64	1.64
H	2.12	1.68	1.52	1.16	0.80	0.80
$\tilde{q}$,$\tilde{g}$	3.55	2.29	1.93	0.25	0.02	$5.9 \cdot 10^{-3}$
$\tilde{\ell}$,$\tilde{\nu}$	28.50	21.28	18.03	10.93	4.33	3.96
$\tilde{\chi}\tilde{\chi}$, $\tilde{q}/\tilde{g}\ \tilde{\chi}$	8.60	5.89	4.4	1.33	0.52	0.40
$tH^{\pm}$	0	0	0	0	0	0
ZZ	48.14	39.37	4.31	0.22	0.07	0.07
$Zb\bar{b}$	3.39	0.96	0.26	0.01	$1.2 \cdot 10^{-3}$	$1.2 \cdot 10^{-3}$
$t\bar{t}$	0.30	0.07	0.06	0.04	$7.3 \cdot 10^{-3}$	$7.3 \cdot 10^{-3}$

Table 5: *Point2 selection results* . From left to right: Process source, cumulative fraction of events (in %) after each (1-6) selection cut, Section 7. For each channel, the fractions of selected events are calculated with respect to the events of each channel, N_{300}^{exp}, given in Tables 2, 3. N_{300}^{exp} are the number of events passing the generation filter described in Section 5.

Process	1	2	3	4	5	6
A	8.37	6.62	4.54	3.24	1.58	1.55
H	8.79	6.56	3.66	2.46	1.06	1.06
$\tilde{q}$,$\tilde{g}$	2.65	1.84	1.40	0.29	0.05	$3.09 \cdot 10^{-3}$
$\tilde{\ell}$,$\tilde{\nu}$	11.83	5.32	5.32	3.55	0.59	0.59
$\tilde{\chi}\tilde{\chi}$, $\tilde{q}/\tilde{g}\ \tilde{\chi}$	7.09	5.27	3.17	1.53	0.69	0.60
$tH^{\pm}$	10.58	8.20	5.91	3.08	1.08	0.92
ZZ	48.14	39.37	4.31	0.22	0.06	0.06
$Zb\bar{b}$	3.39	0.96	0.26	0.01	$1.17 \cdot 10^{-3}$	$1.17 \cdot 10^{-3}$
$t\bar{t}$	0.30	0.07	0.06	0.04	$4.85 \cdot 10^{-3}$	$4.85 \cdot 10^{-3}$

Table 6: *PointA selection results*. From left to right: Process source, cumulative fraction of events (in %) after each (1-7) selection cut, Section 7. For each channel, the fractions of selected events are calculated with respect to the events of each channel, N_{300}^{exp}, given in Tables 2, 3. N_{300}^{exp} are the number of events passing the generation filter described in Section 5.

Process	1	2	3	4	5	6	7
A	4.14	3.34	3.34	1.54	0.38	0.38	0.38
H	1.46	1.23	1.20	0.63	0.17	0.15	0.15
$\tilde{q}$,$\tilde{g}$	2.47	1.54	1.29	0.47	0.09	$9.10 \cdot 10^{-3}$	$4.03 \cdot 10^{-3}$
$\tilde{\ell}$,$\tilde{\nu}$	22.67	16.98	15.16	9.33	1.79	1.60	0.68
$\tilde{\chi}\tilde{\chi}$, $\tilde{q}/\tilde{g}\ \tilde{\chi}$	7.63	5.35	4.21	1.96	0.40	0.20	0.06
$tH^{\pm}$	0.45	0.15	0.13	0.05	0.02	0.02	0
ZZ	48.14	39.37	4.31	0.21	0.04	0.04	$7.37 \cdot 10^{-3}$
$Zb\bar{b}$	3.39	0.96	0.26	0.01	$1.16 \cdot 10^{-3}$	$5.85 \cdot 10^{-4}$	$< 10^{-4}$
$t\bar{t}$	0.30	0.07	0.06	0.04	$3.48 \cdot 10^{-3}$	$3.48 \cdot 10^{-3}$	$1.73 \cdot 10^{-3}$

Table 7: *PointB selection results*. From left to right: Process source, cumulative fraction of events (in %) after each (1-6) selection cut, Section 7. The fraction of events are calculated with respect to the fraction of events of each channel N_{300}^{exp}, given in Tables 2, 3. N_{300}^{exp} are the number of events passing the generation filter described in Section 5.

Process	1	2	3	4	5	6
A	3.45	2.44	1.62	0.96	0.40	0.36
H	5.08	3.85	2.21	1.50	0.66	0.57
$\tilde{q}$,$\tilde{g}$	1.24	0.80	0.62	0.24	0.08	0.03
$\tilde{\ell}$,$\tilde{\nu}$	17.82	14.85	12.87	19.8	0	0
$\tilde{\chi}\tilde{\chi}$, $\tilde{q}/\tilde{g}\ \tilde{\chi}$	3.94	2.93	1.59	0.69	0.20	0.08
$tH^{\pm}$	2.07	1.36	0.88	0.59	0.12	0.06
ZZ	48.14	39.37	4.30	0.22	0.07	0.05
$Zb\bar{b}$	3.39	0.96	0.26	0.01	$1.16 \cdot 10^{-3}$	$1.16 \cdot 10^{-3}$
$t\bar{t}$	0.30	0.07	0.06	0.04	$4.85 \cdot 10^{-3}$	$3.48 \cdot 10^{-3}$

Table 8: *Final samples at the reference points.* From left to right: Process, number of selected events after all selection steps (Section 7) at Point1, Point2, PointA, PointB, for $\int \mathscr{L}\, \mathrm{d}t = 300\ \mathrm{fb}^{-1}$.

Process	Point1	Point2	PointA	PointB
A	30	55	34	7
H	14	36	14	13
$\tilde{q}$,$\tilde{g}$	1	4	39	14
$\tilde{\ell}$,$\tilde{\nu}$	44	1	25	0
$\tilde{\chi}\tilde{\chi}$, $\tilde{q}/\tilde{g}\ \tilde{\chi}$	7	27	13	5
$tH^{\pm}$	0	29	0	1
ZZ	10	8	1	7
$Zb\bar{b}$	2	2	0	2
$t\bar{t}$	79	53	19	45

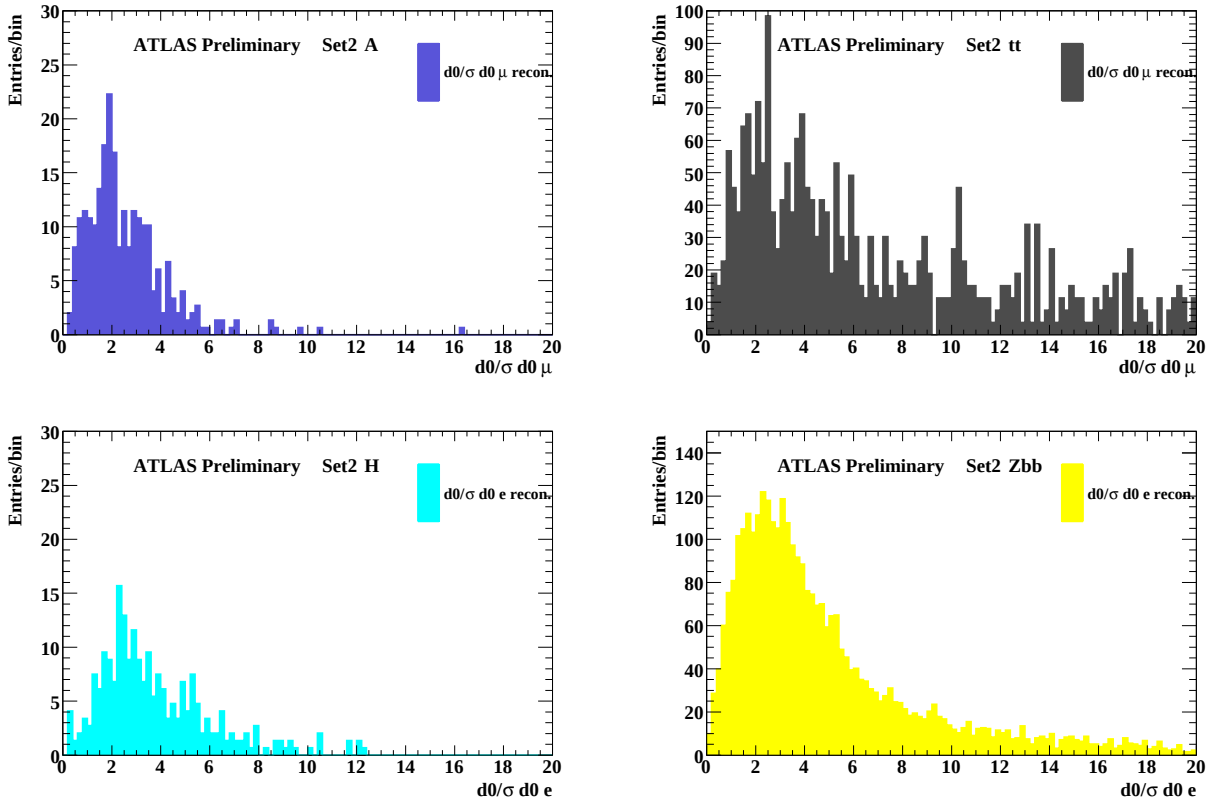

Figure 5: *Point2 selection results.* Reconstructed transverse impact parameter significance, $d0/\sigma_{d0}$, distributions after cut 1, Section 7, for muons in A (top left) and $t\bar{t}$ (top right) events; for electrons in H (bottom left) and $Zb\bar{b}$ (bottom right) events. All distributions are normalized at $\int \mathscr{L}\, dt = 300$ fb^{-1}. Bin width = 0.2.

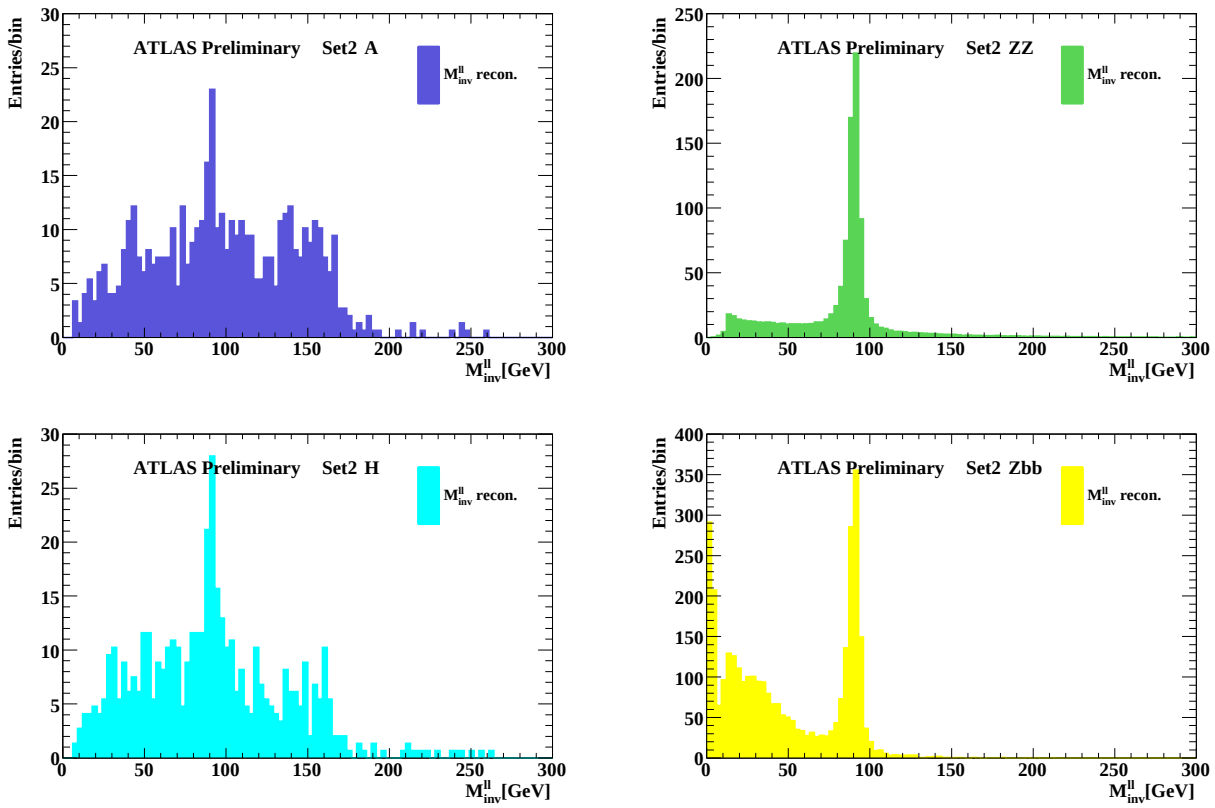

Figure 6: *Point2 selection results.* Reconstructed dilepton invariant mass, $M^{\ell\ell}_{\rm inv}$, distributions after cuts 1,2, Section 7, for A (top left), ZZ (top right), H (bottom left) and $Zb\bar{b}$ (bottom right) events. All distributions are normalized at $\int \mathscr{L}\,{\rm d}t = 300$ fb^{-1}. Bin width = 3 GeV.

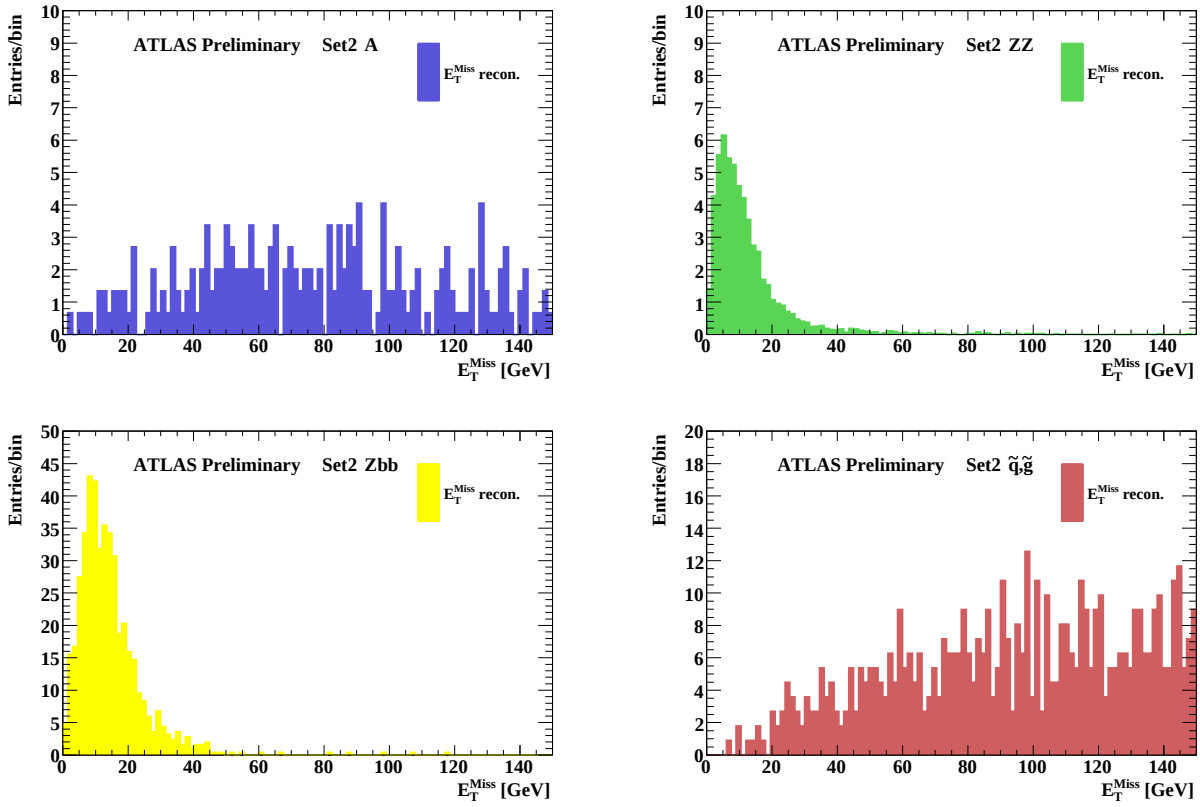

Figure 7: *Point2 selection results.* Reconstructed transverse missing energy, $E_{\mathrm{T}}^{\mathrm{miss}}$, after cuts 1,2,3, Section 7, for A (top left), ZZ (top right), $Zb\bar{b}$ (bottom left), ($\tilde{q}$,$\tilde{g}$) (bottom right) events. All distributions are normalized at $\int \mathscr{L}\,\mathrm{d}t = 300\ \ \mathrm{fb}^{-1}$. Bin width = 1.5 GeV.

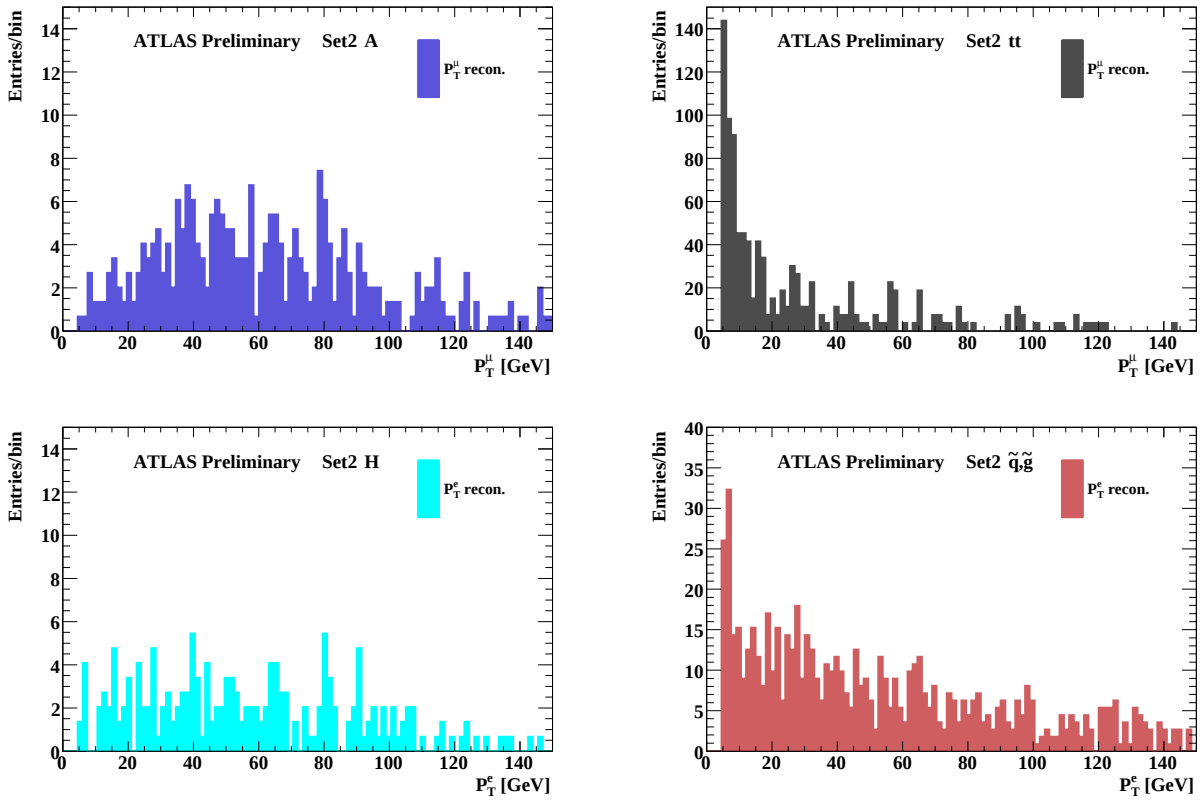

Figure 8: *Point2 selection results.* Reconstructed lepton transverse momentum ($p_T{}^{\mu}$, $p_T{}^{e}$) distributions after cuts 1,2,3,4, Section 7, for muons in A (top left) and $t\bar{t}$ (top right) events; for electrons in H (bottom left) and ($\tilde{q}$,$\tilde{g}$) events (bottom right) events. All distributions are normalized at $\int \mathscr{L}\,dt = 300$ fb^{-1}. Bin width = 1.5 GeV.

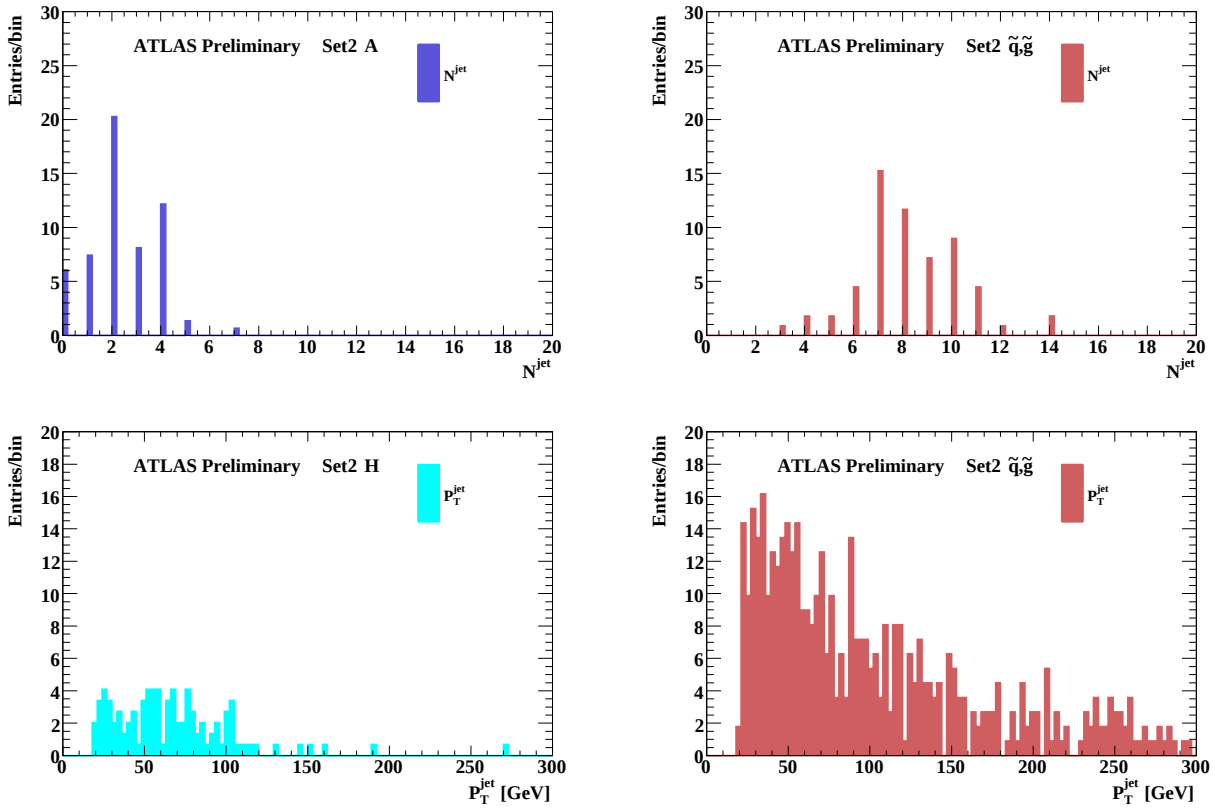

Figure 9: *Point2 selection results.* Reconstructed number of jets, N^{jet}, distributions after cuts 1,2,3,4,5, Section 7, in A (top left) and ($\tilde{q}$,$\tilde{g}$) (top right) events; jet transverse momentum distribution, ${p_T}^{jet}$, in H (bottom left) and ($\tilde{q}$,$\tilde{g}$) (bottom right) events. All distributions are normalized at $\int \mathscr{L}\,dt = 300$ fb^{-1}. ${p_T}^{jet}$ bin width = 1 GeV.

9 Systematic uncertainties

Several quantities used in this analysis are subject to experimental systematic uncertainties. Each systematic effect has been evaluated individually using the given uncertainties on event-by-event basis. These uncertainties are related to the reconstruction of the leptons and the global event activity, as $E_{\mathrm{T}}^{\mathrm{miss}}$ and jet characteristics. Their estimation is based on the method described in Ref. [5], using the ultimate goal performances expected for ATLAS, Ref. [13], downgraded by a conservative factor of two.

The main contributions to systematic uncertainties can be identified as follows:

- For muons the uncertainty on reconstructed p_{T} is $\sigma(1/p_T) = 0.003/p_T \oplus 0.00008$ with p_{T} given in GeV. The uncertainty on transverse momentum scale is estimated $\pm 0.05\%$ and that on the muon identification efficiency is assumed to be 0.1%.

- For electrons the uncertainty on reconstructed E_{T} is $\sigma(E_T) = 0.0050 \times E_T$ with E_{T} in GeV. The uncertainty on the energy scale is estimated $\pm 0.04\%$ and that on the electron identification efficiency is assumed to be 0.04%, flat in E_{T}.

- For jets the uncertainty on jet energy scale is assumed to be $\pm 2\%$; the uncertainty on jet energy resolution is taken $\sigma(E_T) = 0.19 \times \sqrt{E_T}$ with E_{T} in GeV.

- The uncertainty on $E_{\mathrm{T}}^{\mathrm{miss}}$ has been evaluated from jet and lepton uncertainties.

In the evaluation of the systematic effects positive and negative variations are considered separately. The effects of the experimental uncertainties on the yields are summarised in Table 9 for the most relevant supersymmetric processes entering the final (signal and background) samples at Point2. As for the most relevant Standard Model background processes, ZZ and $t\bar{t}$, it turns out that in both cases the systematic uncertainty on the corresponding yield is consistent with zero. Thus we are led to conclude that only negligible systematic uncertainty on the signal significance is expected to arise from the ATLAS detector at its optimum and within the present analysis.

In addition to the effect of systematic mis-measurement on signal efficiency, theoretical uncertainties also limit our ability to estimate the signal efficiency. The major theoretical uncertainties concern the prediction of background cross sections, as described in Ref. [5] and briefly outlined below.

At higher order the cross sections of Standard Model background may become larger by a factor of about 1.5, somewhat depending on the channel, 1.66 for $t\bar{t}$, 1.42 for $Z\bar{b}$, between 1.52 and 1.82 for ZZ. As a result, the Monte Carlo simulation of these processes has to take into account more loops than at LO and need a careful tuning from experimental data.

Many strategies have been developed, based on the combined use of Monte Carlo and data, to allow a realistic evaluation of this background and its systematic uncertainty, for example the ones for ZZ making use of the dilepton invariant mass distribution, with an excellent control region, or the ones for $t\bar{t}$ allowing the selection of a sample dominated by $t\bar{t}$ events. For such considerations see multi-lepton supersymmetry searches, Ref. [5].

The lepton isolation, the calorimeter response and the reconstruction of the missing transverse energy could be affected by pile-up and cavern background.

A pile-up model, for a luminosity of $10^{33}\mathrm{cm}^{-2}\mathrm{s}^{-1}$ and with a cavern background five times higher than expected, was used to determine the degradation of the results, leading to a signal loss of about 14%. However one should keep in mind that at luminosities as high as $10^{34}\mathrm{cm}^{-2}\mathrm{s}^{-1}$ (for which at present no pile-up model is available) the pile-up effect could be more important.

Table 9: *Point2 systematics*. From left to right: source of systematics, percentage change in the selected number of events for signal and supersymmetric background.

Source of systematics	A [%]	H [%]	$tH^{\pm}$ [%]	$\tilde{\ell}, \tilde{\nu}$ [%]	$\tilde{\chi}\tilde{\chi}$, $\tilde{q}/\tilde{g}\,\tilde{\chi}$ [%]
μ efficiency	-	-	-	-	-
μ energy scale $-$	-	$+2.2$	-	-	-
μ energy scale $+$	-	-2.2	-	-	-
μ resolution	-	$+2.2$	$+5.9$	-	-
e efficiency	-1.2	-	-	-	-
e energy scale $-$	-	-	$+2.9$	-	-
e energy scale $+$	-	-	-	-	-
e resolution	-1.2	$+2.2$	$+5.9$	-	$+2.7$
jet energy scale $-$	-	-	-	-	-
jet energy scale $+$	-	-	-	-	-
jet resolution	-	-	-	-	-
missing energy scale $-$	-1.2	$+2.2$	-5.9	-	-
missing energy scale $+$	0	-2.2	-	-	$+2.7$

10 Results and discovery potential

In the following we investigate the domain of parameter space where $A/H \to 4\ell + E_{\mathrm{T}}^{\mathrm{miss}}$ would be detectable for MSSM, Set1 and Set2, and for mSUGRA, SetA and SetB, see Section 3.

The significance of MSSM (mSUGRA) Higgs boson search is given using $\frac{S}{\sqrt{B}}$ as a statistical estimator, where S is the number of signal events (A/H or $A/H/H^{\pm}$), and B the number of background events. A search result of $\frac{S}{\sqrt{B}} \geq 5$ is considered as indication of new physics, instead $\frac{S}{\sqrt{B}} \leq 2$ is exclusion. In another approach, it could be interpreted as discrepancy from Standard Model predictions in the first case or compatibility with them in the second one. In the following, we shall stay with the former interpretation.

The search significance for the A/H neutral Higgs boson is estimated, at two luminosities $\int \mathscr{L}\,\mathrm{d}t$ = 300 fb^{-1} and 100 fb^{-1}, as a function of m_A and tanβ for MSSM, Set1 and Set2; as a function of m_A for mSUGRA, SetA and SetB. Figures 10, 11,12,13 show the discovery and exclusion regions for these sets. The discovery reach presented reflects the choice of parameters in MSSM and mSUGRA frameworks, as shortly shown below. We refer to Ref. [11] for an interesting and comprehensive discussion of these choices and their impact on the results.

Set1 is representative of a parameter region, where most of the signal is produced from $A/H \to \tilde{\chi}_2^0\tilde{\chi}_2^0$. A discovery could be achieved only with the highest luminosity for moderate tanβ values, and in the low m_A region, as shown in Fig. 10. The low m_A edge of the discovery region closely follows the one where the (dominant) $\tilde{\chi}_2^0\tilde{\chi}_2^0$ decay becomes kinematically accessible, $m_A \geq 2 \cdot \mathrm{m}_{\tilde{\chi}_2^0}$ (Table1). The lower tanβ limit is due to the enhancement of the branching ratio $A/H \to t\bar{t}$, at the expenses of $\tilde{\chi}^0$-s branching ratios. For high tanβ values, since the three soft slepton masses for the three generations are degenerate, the number of $\tilde{\chi}$ decays including τ leptons increases, thus reducing drastically the number of decays into electrons and muons.

Set2 corresponds to a parameter region where the signal is originated via heavier -inos, $A/H \to \tilde{\chi}_2^0\tilde{\chi}_3^0$, $\tilde{\chi}_2^0\tilde{\chi}_4^0$, $\tilde{\chi}_3^0\tilde{\chi}_3^0$, $\tilde{\chi}_3^0\tilde{\chi}_4^0$, $\tilde{\chi}_4^0\tilde{\chi}_4^0$ and $A/H \to \tilde{\chi}_1^{\pm}\tilde{\chi}_2^{\pm}$, $\tilde{\chi}_2^{+}\tilde{\chi}_2^{-}$. The discovery reach is shown in Fig. 11. There are two separated discovery regions, a smaller region at low values of tanβ and m_A, dominated by $A/H \to \tilde{\chi}_2^0\tilde{\chi}_2^0$, and a larger one at higher m_A values up to tanβ = 50. The lower m_A edge of the larger discovery

region closely follows that where heavier neutralino decays become kinematically accessible, Table 1. In the smaller region the branching ratio of A/H into $\tilde{\chi}_2^0\tilde{\chi}_2^0$ ($\tilde{\chi}_2^0 \to \tilde{\chi}_1^0\ell^+\ell^-$) is larger than the one of $A/H \to t\bar{t}$, in contrast with Set1.

The difference in discovery regions between Set1 and Set2 is mainly due to the different slepton masses, the stau mass in Set2 is 100 GeV above the other slepton masses (Section 3). Then, decays into electrons and muons become possible extending the discovery region to higher values of $\tan\beta$, and the A/H discovery can be reached with Set2 parameters also at the lower luminosity $\int \mathscr{L}\,\mathrm{d}t = 100\ \mathrm{fb}^{-1}$. For high m_A values, the discovery region for Set2 is significantly wider than for Set1. In Set2, the mass difference between $\tilde{\chi}_3^0$ or $\tilde{\chi}_4^0$ and $\tilde{\chi}_1^0$ exceeds the Z mass, allowing their decay into $\tilde{\chi}_1^0$ via on-mass-shell Z. This is not the case in Set1, where the $\tilde{\chi}_2^0$ is not heavy enough to decay via an on-mass-shell Z into $\tilde{\chi}_1^0$. Consequently, a large portion of signal events are rejected by the dilepton invariant mass cut in Set2, but not in Set1.

Another interesting advantage of Set2 resulting from Table 8, is that the signal search can be extended to the charged sector of MSSM Higgs bosons. This includes charged Higgs decays into chargino and neutralino channels producing four leptons (three from neutralino/chargino) and a number of undetectable particles in the final state. Then, the $tH^\pm$ events can be grouped with the signal rather than with the background, despite that this analysis is not designed for these events. The results on the $H^\pm$ boson search combined with the results from the A/H search enlarge the discovery range (Fig. 12). By including charged Higgs bosons, the MSSM Higgs boson discovery reach with Set2 parameters is high also for the lower luminosity, $\int \mathscr{L}\,\mathrm{d}t = 100\ \mathrm{fb}^{-1}$.

For the two mSUGRA scenarios identified as SetA and SetB, the significance, $\frac{S}{\sqrt{B}}$, of the A/H neutral Higgs boson search, as a function of m_A is shown in Fig. 13. SetA is dominated by $A/H \to \tilde{\chi}_2^0\tilde{\chi}_2^0$, SetB by heavier $\tilde{\chi}$ decays. In the SetA configuration the discovery reach, blue line in Fig. 13 (left), is reached at m_A values > 266 GeV in the higher luminosity scenario. A mass range of $266 - 274$ GeV is accessible also in the lower luminosity scenario. The SetB perspective is more restricted, allowing only for exclusion and not for discovery.

With respect Ref. [11], the results outlined above, despite the presence of some differences, confirm the possibility of a discovery of A/H decays in $4\ell + E_{\mathrm{T}}^{\mathrm{miss}}$ final state via a pair of $\tilde{\chi}^0$'s. The discovery regions obtained in this analysis are reduced both in m_A and in $\tan\beta$ but have the same shape and same threshold in m_A, determined by kinematics. The same features are reflected in the Set2 results, where two separate regions are present but with narrow areas. A lower significance is obtained for mSUGRA points.

These differences may be explained by two main reasons: a) the use in the analysis of detector full simulation, which has a relevant impact on many physics quantities, as momentum, energy, missing transverse energy and lepton isolation; b) detailed inclusion of $t\bar{t}$ background. Other differences in the analysis may come from the use of a different significance estimator, and a possible difference in Standard Model processes cross sections.

The discovery regions for neutral supersymmetric Higgs bosons decaying into Standard Model particles [4–6] are obtained with MSSM/mSUGRA parameters different from the ones used in this analysis: a choice was made to depress the Higgs boson decays into sparticles. Consequently, the discovery regions for Higgs bosons decaying into Standard Model particles can not be easily compared with the ones including decays into supersymmetric particles.

11 Conclusions

The discovery potential of the ATLAS experiment at LHC was investigated for A/H decays into sparticles involving light neutralinos $\tilde{\chi}_2^0\tilde{\chi}_2^0$, heavier neutralinos $\tilde{\chi}_2^0\tilde{\chi}_3^0$, $\tilde{\chi}_2^0\tilde{\chi}_4^0$, $\tilde{\chi}_3^0\tilde{\chi}_3^0$, $\tilde{\chi}_4^0\tilde{\chi}_4^0$ and charginos $\tilde{\chi}_1^\pm\tilde{\chi}_2^\pm$,

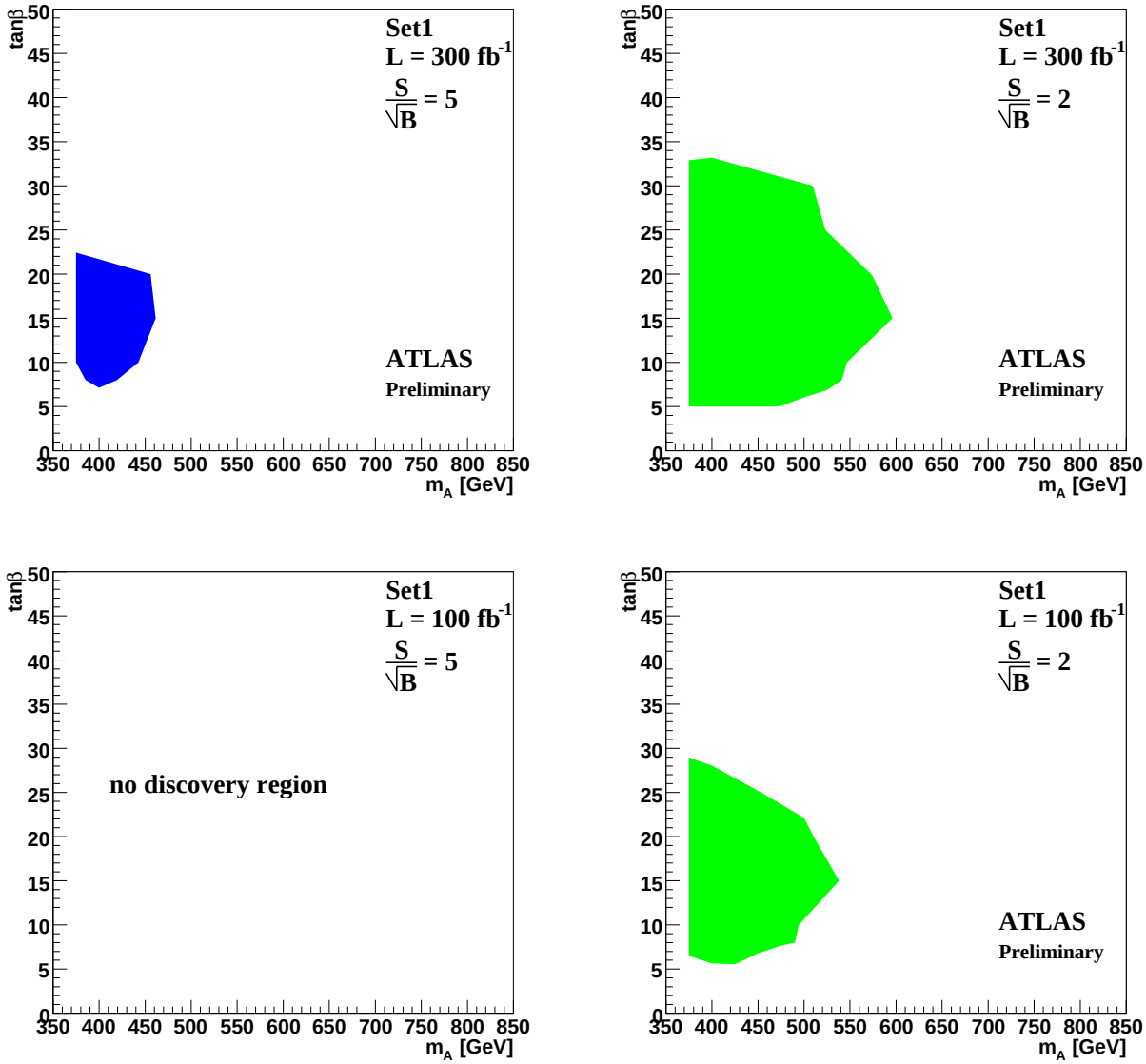

Figure 10: *Set1*. Discovery potential for a neutral Higgs boson A/H of mass m_A decaying to four leptons accompanied by missing transverse energy, as a function of m_A: contours are drawn for a search significance $\frac{S}{\sqrt{B}} = 5$ (left) and $\frac{S}{\sqrt{B}} = 2$ (right), with an integrated luminosity of $\int \mathscr{L}\,dt = 300$ fb^{-1} (top) and 100 fb^{-1} (bottom). No discovery region is found for this latter luminosity. S is the number of signal events, B is the number of background events.

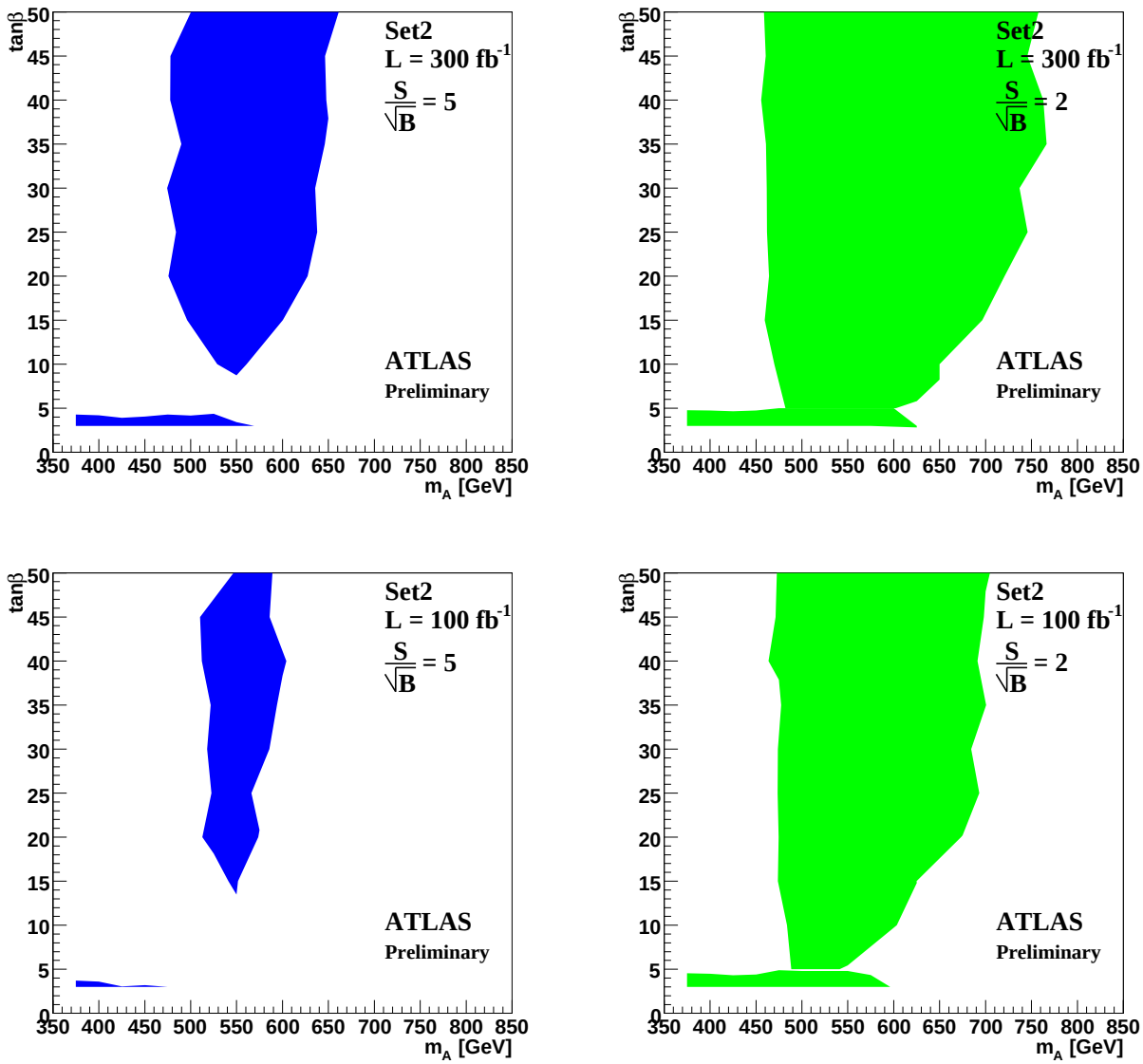

Figure 11: *Set2.* Discovery potential for a neutral Higgs boson A/H of mass m_A decaying to four leptons accompanied by missing transverse energy, as a function of m_A: contours are drawn for a search significance $\frac{S}{\sqrt{B}} = 5$ (left) and $\frac{S}{\sqrt{B}} = 2$ (right), with an integrated luminosity of $\int \mathscr{L}\,\mathrm{d}t = 300$ fb^{-1} (top) and 100 fb^{-1}(bottom). S is the number of signal events, B is the number of background events.

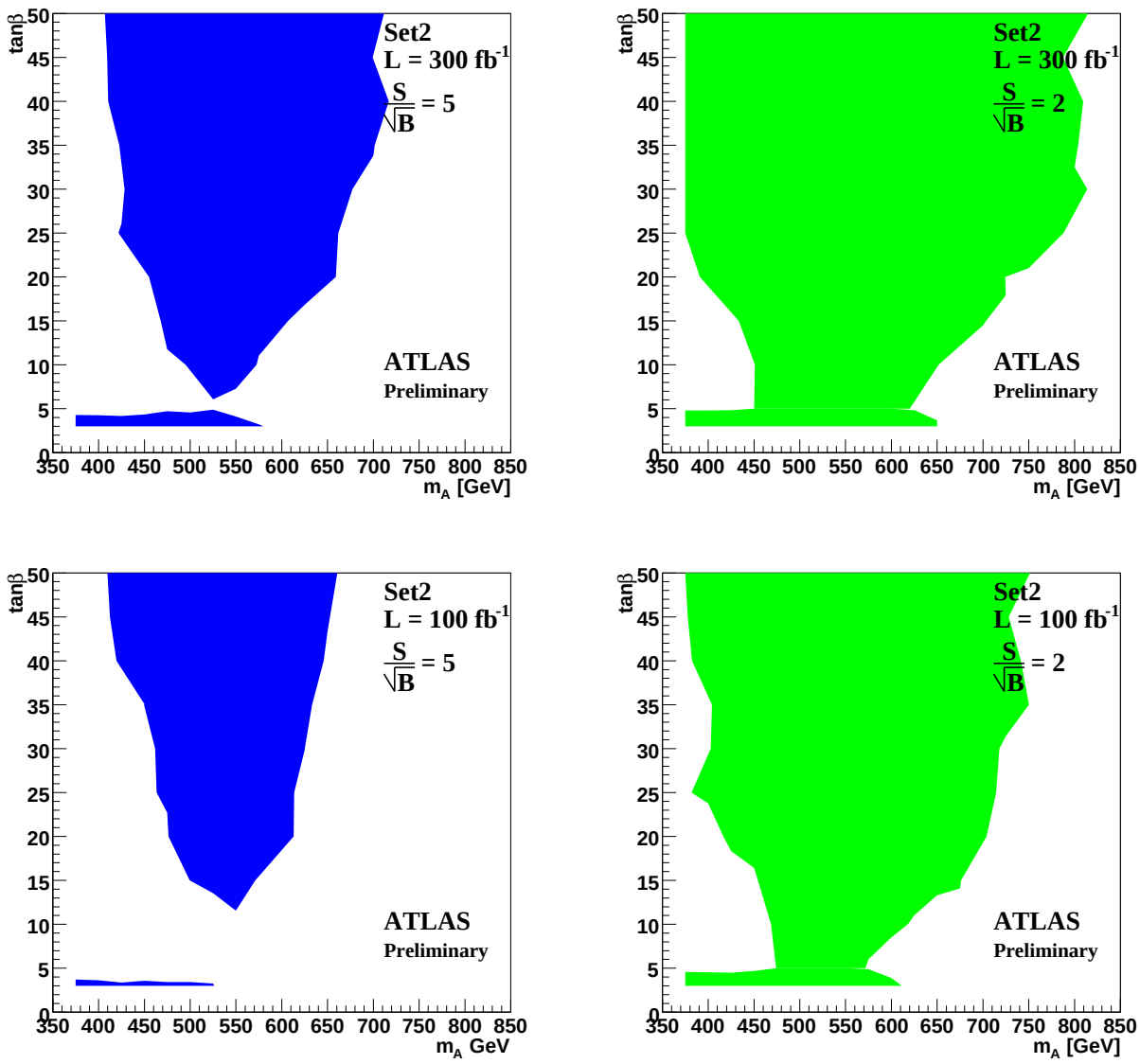

Figure 12: *Set2 including* $H^{\pm}$. Discovery potential for a Higgs boson $A/H/H^{\pm}$ of mass m_A decaying to four leptons accompanied by missing transverse energy, as a function of m_A: contours are drawn for a search significance $\frac{S}{\sqrt{B}} = 5$ (left) and $\frac{S}{\sqrt{B}} = 2$ (right), with an integrated luminosity of $\int \mathscr{L}\,dt = 300$ fb^{-1} (top) and 100 fb^{-1} (bottom). S is the number of signal events, B is the number of background events.

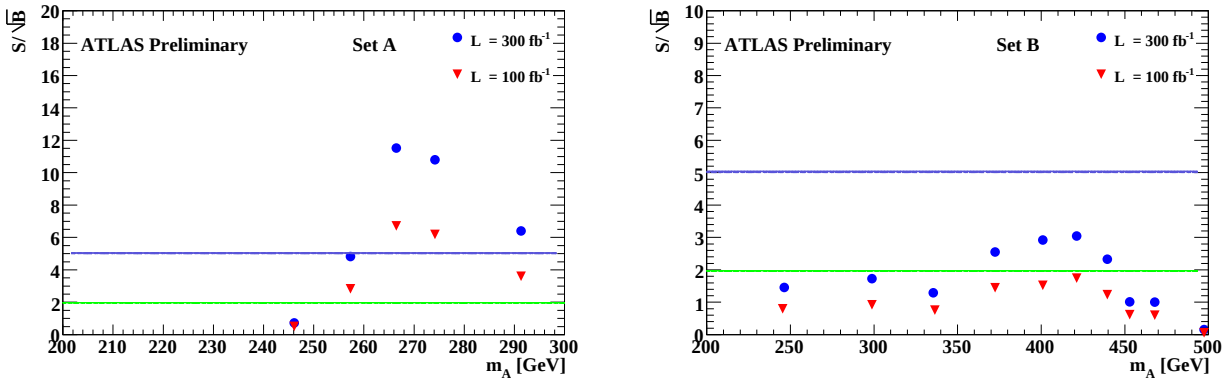

Figure 13: *SetA, SetB.* Discovery potential for a Higgs boson A/H of mass m_A decaying to four leptons accompanied by missing transverse energy, as a function of m_A, for mSUGRA SetA (right) and SetB (left): values of the search significance, $\frac{S}{\sqrt{B}}$, with an integrated luminosity of $\int \mathscr{L}\,dt = 300$ fb^{-1}(blue bullet) and 100 fb^{-1} (red triangle). The blue and green lines correspond to a search significance $\frac{S}{\sqrt{B}} = 5$ and $\frac{S}{\sqrt{B}} = 2$, respectively. S is the number of signal events, B is the number of background events.

$\tilde{\chi}_2^+\tilde{\chi}_2^-$, with the subsequent decay $\tilde{\chi}_2^0 \to \tilde{\chi}_1^0\ell^+\ell^-$. We considered a final state with four leptons accompanied by missing energy. The study has been performed using a realistic detector simulation of signal and background in a large range of (tanβ, m_A) parameters.

The branching ratio of A and H into four leptons is determined by the interplay between a number of MSSM (mSUGRA) parameters leading to different results in this search. The four sets of parameters investigated, two for MSSM and two for mSUGRA, Ref. [11], are dominated by light neutralino decays (Set1, SetA) or by heavier $\tilde{\chi}$ decays (Set2, SetB). In the higher luminosity scenario, $\int \mathscr{L}\,dt = 300$ fb^{-1}, a signal may be detected in three of the four sets; in two of them discovery may be reached also with a lower integrated luminosity, 100 fb^{-1}.

12 Acknowledgements

This work originated from a discussion of one of the authors with prof. Stefano Moretti. His help and advise in the starting phase are here gratefully acknowledged.

References

[1] ALEPH, DELPHI, L3, OPAL Collaboration, *Phys. Lett.* **B565** (2003) 61.

[2] ALEPH, DELPHI, L3, OPAL Collaboration, *Eur. Phys. J.* **C47** (2006) 547.

[3] ALEPH, DELPHI, L3, OPAL Collaboration, *Search for charged Higgs bosons: Preliminary combined results using LEP data collected at energies up to 209 GeV* hep-ex/010703 (2001).

[4] ATLAS Collaboration, *ATLAS detector and Physics Performance: Technical Design Report*, Volume 2, report CERN/LHCC/99-15 (1999).

[5] ATLAS Collaboration, *Expected Performance of the ATLAS Experiment - Detector, Trigger and Physics* arXiv:0901.0512 (2009).

[6] CMS Collaboration, *CMS detector and Physics Performance: Physics Technical Design Report*, Volume 1, report CERN/LHCC/2006-001 (2006).

[7] F. Moortgat, S. Abdullin, and D. Denegri, *Observability of MSSM Higgs bosons via sparticle decay modes in CMS* hep-ph/0112046 (2001).

[8] M. Bisset, F. Moortgat, and S. Moretti, *Eur. Phys. J.* **C30** (2003) 419.

[9] C. Charlot, R. Salerno, and Y. Sirois, *J. Phys.* **G34** (2007) N1.

[10] C. Hansen, N. Gollub, K. Assamagan, and T. Ekelof, *Eur. Phys. J.* **C44S2** (2005) 1.

[11] M. Bisset, J. Li, N. Kersting, F. Moortgat, and S. Moretti, *Four-lepton LHC events from MSSM Higgs boson decays into neutralino and chargino pairs* hep-ph/0709.1029 (2007).

[12] S. Gentile, *ATLAS MSSM Higgs search in SUSY cascade*, ATL-PHYS-PROC-2008-077, CERN, Geneva, November, 2009.

[13] ATLAS Collaboration, *JINST* **3** (2008) S08003.

[14] A. Djouadi, *Phys. Rep.* **459** (2008) 1.

[15] S. P. Martin, *A supersymmetry primer* hep-ph/9709356 (1997).

[16] H. E. Haber and G. L. Kane, *Phys. Rep.* **117** (1985) 75.

[17] C. Amsler *et. al.*, *Phys. Lett.* **B667** (2008) 1.

[18] H.-P. Nilles, *Phys. Rep.* **110** (1984) 1.

[19] H. Baer, F. E. Paige, S. D. Protopopescu, and X. Tata, *ISAJET 7.69: A Monte Carlo Event Generator for pp, $\bar{p}p$, and e^+e^- Reactions* hep-ph/0312045 (2003).

[20] S. Agostinelli *et. al.*, *Nucl. Instrum. Meth.* **A506** (2003) 250.

[21] G. Corcella *et. al.*, *JHEP* **1** (2001) 10.

[22] J. M. Butterworth, J. R. Forshaw, and M. H. Seymour, *Z. Phys.* **C72** (1996) 637.

[23] S. Frixione and B. R. Webber, *JHEP* **06** (2002) 29.

[24] T. Sjostrand, S. Mrenna, and P. Skands, *JHEP* **05** (2006) 26.

[25] B. P. Kersevan and E. Richter-Was, *Comput. Phys. Commun.* **149** (2003) 142.